European Journal of Medicinal Chemistry 76 (2014) 125–131

Contents lists available at ScienceDirect

European Journal of Medicinal Chemistry

journal homepage: http://www.elsevier.com/locate/ejmech

Short communication

Homoisoflavonoids as potential imaging agents for β-amyloid plaques in Alzheimer's disease

Changsheng Gan [a,*], Zhenzhen Zhao [a], Dou-Dou Nan [b], Binbin Yin [a], Jingyi Hu [a]

[a] Engineering Research Center of Bio-process of Ministry of Education, Hefei University of Technology, Hefei, Anhui 230009, PR China
[b] CAS Key Laboratory of Brain Function and Disease, School of Life Sciences, University of Science and Technology of China, Hefei, Anhui 230027, PR China

ARTICLE INFO

Article history:
Received 7 November 2013
Received in revised form
31 December 2013
Accepted 8 February 2014
Available online 11 February 2014

Keywords:
Alzheimer's disease
Amyloid
Imaging agent
Homoisoflavonoid
Binding assay

ABSTRACT

A series of homoisoflavonoids [(*E*)-3-benzylidenechroman-4-ones, **3a**–**l**] as novel potential diagnostic imaging agents targeting β-amyloid (Aβ) plaques in Alzheimer's disease (AD) were synthesized and evaluated. In vitro binding studies using $A\beta_{1-40}$ aggregates with [^{125}I]IMPY as the reference ligand showed that these compounds demonstrated high to low binding affinities at the K_i values ranged from 9.10 to 432.03 nM, depending on the substitution of the phenyl ring. Fluorescent staining in vitro indicated that one compound with a *N*,*N*-dimethylamino group intensely stained Aβ plaques within brain sections of postmortem AD patients. Biodistribution studies in normal mice after i.v. injection of the radioiodinated homoisoflavonoid displayed good initial brain uptake (2.61% ID/g at 2 min post-injection) and rapid clearance from the brain (0.18% ID/g at 60 min), which is desirable for amyloid imaging agents. The results strongly suggest that these derivatives are worthy of further study and may be useful amyloid imaging agents for early detection of amyloid plaques in the brain of AD.

1. Introduction

Alzheimer's disease (AD) is a progressive neurodegenerative disorder and a leading cause of dementia [1–3]. Clinical symptoms of AD include cognitive decline, irreversible memory loss, disorientation, language impairment, etc. Although great progress has been made towards understanding the disease mechanisms in the last three decades, there remains no cure for AD. The current medications, including donepezil, galantamine, rivastigmine and memantine are primarily symptomatic treatments [4]. Early intervention may delay the onset or progression of AD. It has been well established that the major neuropathological characteristic of AD is the presence of senile plaques (SPs), which are composed of β-amyloid (Aβ) protein aggregates, and neurofibrillary tangles (NFTs), which are highly phosphorylated tau proteins [5,6]. The amyloid cascade hypothesis indicates that the deposition of amyloid plaques constitutes a central and probably early event in the pathogenesis of AD. Therefore, the monitoring of Aβ plaques would be beneficial for the diagnosis, staging, and treatment of AD.

The development of amyloid-specific imaging agents is generally based on conjugated dyes, such as Congo red, Chrysamine G, and thioflavin-T, which have been used in fluorescent staining of plaques and tangles in postmortem AD brain sections. Several radioligands for positron emission tomography (PET) and single photon emission computerized tomography (SPECT), including [^{11}C]PIB (2-(4-(methylamino)phenyl)-6-hydroxybenzothiazole, Pittsburgh compound B) [7–9], [^{11}C]SB-13 (4-*N*-methylamino-4′-hydroxystilbene) [10], [^{11}C]AZD2184 (2-(6-(methylamino)pyridin-3-yl)-1,3-benzothiazol-6-ol) [11], [^{18}F]FDDNP (2-(1-(6-(2-fluoroethyl)-methylamino)-2-naphthyl)ethylidene)malononitrile)) [12,13], [^{18}F]GE067 (2-(3′-fluoro-4′-(methylamino)phenyl)-6-hydroxybenzothiazole) [14], [^{18}F]BAY94-9172 (4-(*N*-methylamino)-4′-(2-(2-(2-fluoroethoxy)ethoxy)ethoxy)stilbene) [15], [^{18}F]AV-45 ((*E*)-4-(2-(6-(2-(2-(2-fluoroethoxy)ethoxy)ethoxy)pyridin-3-yl)vinyl)-*N*-methylbenzenamine) [16,17], and [^{123}I]IMPY (2-(4′-dimethylaminophenyl)-6-iodoimidazo[1,2-α]pyridine) [18], [^{11}C] BF-227 (2-(2-(2-Dimethylaminothiazol-5-yl)ethenyl)-6-(2-fluoroethoxy)benzoxazole) [19], have been tested in clinical trials and demonstrated the potential utility as in vivo imaging agents for Aβ plaque deposition in the living human brain (Fig. 1).

To date, [^{11}C]PIB, the most widely studied amyloid probe, is limited by the 20-min radioactive decay half-life of ^{11}C for routine clinical use. To overcome the limitation, there are now several amyloid probes labeled with ^{18}F (110-min radioactive decay half-life) under clinical development, such as [^{18}F]BAY94-9172, ^{18}F-Florbetapir ([^{18}F]AV-45), and [^{18}F]3′-F-PIB [20]. There are still

* Corresponding author.
E-mail address: gancs7894@163.com (C. Gan).

http://dx.doi.org/10.1016/j.ejmech.2014.02.020
0223-5234/

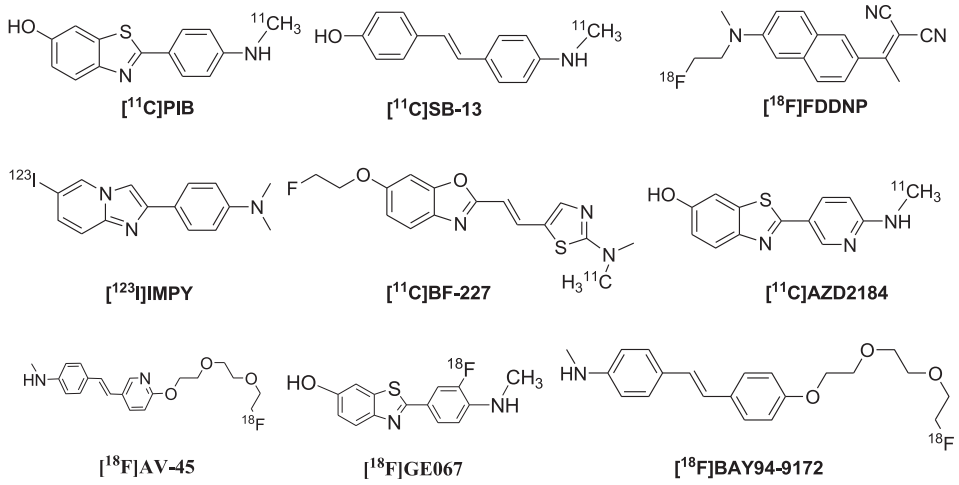

Fig. 1. Chemical structures of representative amyloid imaging agents.

some limitations of these probes, such as the higher white matter non-specific binding than [^{11}C]PIB [21,22]. [^{123}I]IMPY [18,23–26], the first SPECT probe to be evaluated in human, displayed a poor signal-to-noise ratio. Therefore, there is still a need to develop more probes for the imaging of AD brain SPs.

It is well known flavonoid is one of the most important natural products with a variety of physiological activities. Heo's results indicated that quercetin, one of the major flavonoids in some fruits and vegetables, contributed significantly to the protective effects of neuronal cells against oxidative stress-induced neurotoxicity from AD [27]. And the effects of polyhydroxyflavones on the formation, extension, and destabilization of Aβ aggregates were studied in vitro [28]. These flavones could inhibit the formation of Aβ aggregates, as well as destabilizing preformed Aβ aggregates, and some amyloid imaging agent based on the structure of flavone were developed by Ono et al. [29,30].

Homoisoflavonoids constitute a small class of natural products prevalently isolated from the bulbs, rhizomes, or roots of several genera of *Hyacinthaceae* and *Caesalpinioideae*. Several natural and synthetic homoisoflavonoids, like the related flavonoids, were found to possess various biological properties such as antifungal [31], antiviral [32], antimutagenic [33], antioxidant [34], anti-allergic and antihistaminic [35], anti-inflammatory [36], protein tyrosine kinase inhibitor activities [37], monoamine oxidase and cholinesterase inhibitor activities [38,39]. In the present study, a series of homoisoflavonoids as flavonoid derivatives or hybrids of flavone and chalcone structure, were synthesized and evaluated as amyloid imaging agents. The results indicated that some compounds, which can be further radiolabeled by C-11, F-18 or I-123 [40–42], may be developed into potential useful amyloid imaging agents for in vivo detecting β-amyloid plaques in the brain of AD.

2. Results and discussion

2.1. Chemistry

As shown in Scheme 1, the homoisoflavonoids were readily prepared by direct condensation of chroman-4-one and different benzaldehyde. These compounds except **3l** were generally synthesized by heating chroman-4-one with corresponding benzaldehyde in saturated phosphorous acid [38]. In the case of **3l**, chroman-4-one was reacted with the corresponding benzaldehyde in HOAc and saturated hydrochloride acid at room temperature to produce **3l** [43]. Compound **3f** was prepared by heating **3e** in ethanol under the catalysis of $SnCl_2 \cdot 2H_2O$. The *trans*-configuration of compounds **3a**–**l** was confirmed by the chemical shift of the vinyl proton in ^{1}H NMR. Because of the deshielding effect resulting from the neighboring carbonyl group, the vinyl proton gave a higher chemical shift in the *trans*-isomer (>7 ppm) than the *cis*-isomer [44].

The radioiodinated form of compound **3d** was prepared from the corresponding tributyltin precursor by an iododestannylation. As shown in Scheme 2, the corresponding tributyltin derivative **3m** was synthesized from **3d** by reacting with bis(tributyltin) and

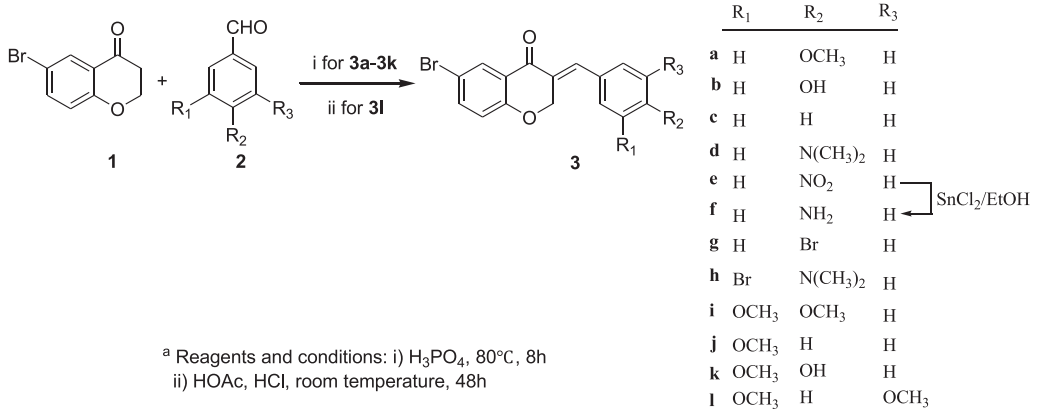

	R_1	R_2	R_3
a	H	OCH_3	H
b	H	OH	H
c	H	H	H
d	H	$N(CH_3)_2$	H
e	H	NO_2	H
f	H	NH_2	H
g	H	Br	H
h	Br	$N(CH_3)_2$	H
i	OCH_3	OCH_3	H
j	OCH_3	H	H
k	OCH_3	OH	H
l	OCH_3	H	OCH_3

[a] Reagents and conditions: i) H_3PO_4, 80°C, 8h
ii) HOAc, HCl, room temperature, 48h

Scheme 1. Synthesis of **3a**–**3l**.

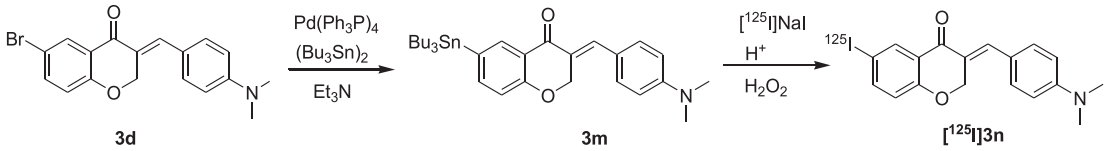

Scheme 2. Synthesis of **3m** and [^{125}I]**3n**.

$Pd(PPh_3)_4$ in Et_3N at 80 °C, and then reacted with [^{125}I] sodium iodide, hydrogen peroxide to produce radioiodinated product [^{125}I] **3n** [43].

2.2. In vitro binding assay

The binding affinities (K_i) of the homoisoflavonoids for $A\beta_{1-40}$ aggregates were determined by competition binding assay with [^{125}I]IMPY as radioligand, while IMPY was also screened using the same system for comparison. [^{125}I]IMPY was prepared as described previously [25]. The results were shown in Table 1.

In the compounds **3a**–**3l**, when the substituents were changed, the inhibition constant (K_i) values exhibited great variations. In the case of *para*-substitution of the right phenyl ring, compound **3a** ($R_2 = OCH_3$) and **3d** ($R_2 = NMe_2$) displayed a higher binding affinity ($K_i = 9.98 \pm 0.81$ nM, 9.10 ± 1.11 nM, respectively) than the others, which is slightly superior to that of IMPY ($K_i = 13.65$ nM). However, the replacement of these substituents with NO_2 group resulted in a steep decrease in the binding affinity (for **3e**, $K_i = 107.60$ nM)(*E*)-3-benzylidene-6-bromo-chroman-4-one (**3c**) without any substituents on the right phenyl ring also showed poor affinity ($K_i = 103.62$ nM). These suggest that the phenyl rings should be electron rich in order for these compounds to exhibit high binding affinities, possibly due to their stronger π–π stacking with amyloid peptides. The introduction of Br at the *ortho* position of **3d** resulted in a slight reduction of binding affinity (for **3h**, $K_i = 25.54$ nM). From the K_i values of **3i**–**3l**, we can see that changing the substituent site and substituent number can also affect the bind affinity (for **3i**, **3j** and **3l**, $K_i = 54.22$, 73.46 and 39.19 nM, respectively), which are all lower than that of **3a** with only one *para*-substituted OCH_3 group. These results imply that the steric hindrance may lead to the reduction of the binding properties.

2.3. AD brain tissue fluorescent staining

Since these homoisoflavonoids could emit fluorescence well, the AD brain tissue fluorescent staining was further performed for visually investigating the binding ability of these compounds to the senile plaques (SPs) in vitro. As shown in Fig. 2, almost all the SPs in the brain section could be labeled by ligand **3d** (B1), as confirmed by staining with ThS (A1) in adjacent sections compared with the blank control sections (C1). The details of the SPs staining were clearly visualized by the fluorescence of **3d** (B2). Unlike ThS (A2), the NFTs couldn't be labeled by **3d** (A2, B2).

Table 1
Inhibition constants (K_i) of homoisoflavonoids on [^{125}I]IMPY binding to $A\beta_{1-40}$ aggregates.

Compound	R_1	R_2	R_3	K_i[a]
3a	H	OCH_3	H	9.98 ± 0.81
3b	H	OH	H	103.35 ± 11.80
3c	H	H	H	103.62 ± 14.53
3d	H	$N(CH_3)_2$	H	9.10 ± 1.11
3e	H	NO_2	H	107.60 ± 14.28
3f	H	NH_2	H	63.57 ± 10.07
3g	H	Br	H	143.81 ± 7.28
3h	Br	$N(CH_3)_2$	H	25.54 ± 2.32
3i	OCH_3	OCH_3	H	54.22 ± 3.11
3j	OCH_3	H	H	73.46 ± 9.49
3k	OCH_3	OH	H	432.03 ± 64.64
3l	OCH_3	H	OCH_3	39.19 ± 7.93
IMPY				13.65 ± 0.93

[a] Each value was determined in three separate experiments with duplicate measurements each time.

2.4. Radioiodination

The synthesis of the tributyltin precursors (**3m**) and corresponding [^{125}I]-labeled compounds **3n** are shown in Scheme 2. Standard iododestannylation reactions, using [^{125}I] sodium iodide, hydrogen peroxide and hydrochloric acid were conducted successfully [25,43]. Purification of the radiolabeled compounds was performed by HPLC (Column: Waters Symmetry C18, 4.6 × 250 mm, 5 μm; Mobile phase: MeOH/H_2O = 8/2; Flow rate = 1.0 mL/min; Bioscan Flow-Count FC-3100 Na/I PMT based radioactivity detector). The final product [^{125}I]**3n** showed greater than 95% radiochemical purity with high specific activity (2200 Ci/mmol).

2.5. Biodistribution in normal mice

Biodistribution experiments were performed in normal mice in order to evaluate the pharmacokinetic properties of these derivatives. [^{125}I]**3n** was injected intravenously into normal ICR mice for biodistribution studies. As shown in Table 2, the initial brain uptake was 2.61% ID/g at 2 min postinjection, indicating an efficient BBB permeability, sufficient for brain imaging probe. In addition, it displayed rapid clearance from the normal brain with 0.32% and 0.18% ID/g at 30 min and 60 min postinjection, respectively. The ratio of 60 min–2 min brain uptake values for the ligand was 6.9%.

3. Conclusions

In conclusion, we have synthesized and evaluated a series of the homoisoflavonoid derivatives as novel potential imaging probes for β-amyloid plaques in AD brain. In particular, compounds **3a** and **3d** exhibited high binding affinities to amyloid plaques in the nanomolar range and **3d** could selectively label the amyloid plaques within brain sections of postmortem AD patients by tissue fluorescent staining. In the biodistribution studies using normal ICR mice, [^{125}I]**3n** displayed a good brain penetration and fast washout from the brain, highly desirable characteristics for in vivo amyloid imaging agents. Taken together, the present results suggest that the homoisoflavonoid derivatives may be useful probes for detecting amyloid plaques in the AD brain.

4. Experimental section

4.1. Materials and instruments

The reagents used in the syntheses were purchased from Alfa Aesar, Sigma–Aldrich and Sinopharm Chemical Reagent Co. Ltd and were used without further purification unless otherwise indicated. [^{125}I]NaI (2200 Ci/mmol) was purchased from PerkinElmer Life and

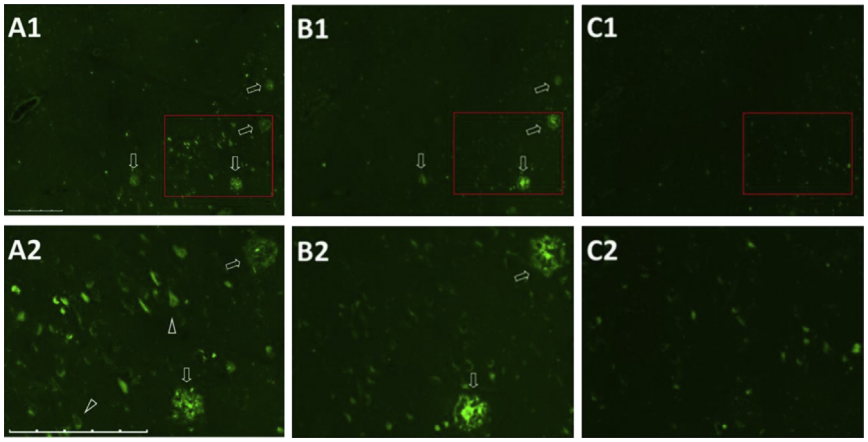

Fig. 2. Three adjacent AD brain sections were stained (A: ThS, B: **3d**, C: blank control). The hollow arrows indicate the amyloid plaques. The triangle arrows indicate the neurofibrillary tangles. The bottom row was the magnified images of the boxed area in the top row. Bar = 250 μm.

Analytical Sciences (USA). The AD human paraffin brain sections were obtained from the Netherlands brain bank (coordinator: Dr. I. Huitinga). The NMR spectra were obtained on Agilent VNMRS-600 (600 MHz) for compound **3d**, **3h** and Bruker Avance-300 (300 MHz) spectrometer for other compounds with TMS as the internal standard. Melting points were determined using capillary tubes with YRT-3 apparatus. High-resolution MS were obtained on a Micromass GCT mass spectrometer. FT-IR spectra were obtained on a Thermo Scientific Nicolet 8700 system.

4.2. Chemistry

Typical procedure for the synthesis of **3a**–**3e** and **3g**–**3k**: To a stirring solution of substituted benzaldehyde (0.5 mmol) in 85% phosphorous acid (8 mL) was added 6-bromochroman-4-one (0.5 mmol). The mixture was stirred at 80 °C for 8 h. After cooling, the mixture was diluted with water (and made alkaline for the preparation of compound **3d** and **3h**). The precipitate was separated by vacuum filtration and washed with cold water and recrystallized from EtOH or purified by silica gel chromatography (6:1 petroleum ether/ethyl acetate).

4.2.1. (E)-3-(4-Methoxybenzylidene)-6-bromo-chroman-4-one (*3a*)

Yellow solid, mp 155–156 °C. Yield: 86%. ^{1}H NMR ($CDCl_3$) δ 8.12 (s, 1H, H-5), 7.84 (s, 1H, =CHPh), 7.55 (d, 1H, J = 8.6 Hz, H-7), 7.29–7.26 (m, 2H, H-2′, H-6′), 6.98 (d, 2H, J = 7.9 Hz, H-3′, H-5′), 6.87 (d, 1H, J = 8.6 Hz, H-8), 5.37 (s, 2H, H-2), 3.87 (s, 3H, OMe). ^{13}C NMR ($CDCl_3$) δ 181.1, 161.1, 160.0, 138.4 (2C), 132.4, 130.5, 128.1, 127.0, 123.6, 120.1, 114.7, 114.6, 68.1, 55.6. HRMS: calcd for $C_{17}H_{13}^{79}BrO_3$ $[M]^+$ 344.0048, found 344.0053, calcd for $C_{17}H_{13}^{81}BrO_3$ $[M]^+$ 346.0028, found 346.0031. IR (KBr, cm^{-1}) γ 2955, 2835, 1661, 1600, 1263, 1030, 819.

Table 2
Biodistribution in normal mice after intravenous injection of [^{125}I]**3n** (% ID/g, n = 5, mean ± SD).

Organ	2 min	10 min	30 min	1 h	2 h
Blood	8.35 ± 1.46	3.87 ± 0.94	2.38 ± 1.33	1.22 ± 0.47	1.05 ± 0.46
Brain	2.61 ± 0.51	0.83 ± 0.05	0.32 ± 0.05	0.18 ± 0.02	0.10 ± 0.02
Heart	4.46 ± 1.13	1.87 ± 0.21	0.87 ± 0.16	0.49 ± 0.02	0.36 ± 0.06
Liver	13.57 ± 1.84	4.71 ± 0.33	2.07 ± 0.34	1.23 ± 0.10	1.05 ± 0.26
Spleen	2.54 ± 0.23	1.27 ± 0.14	0.70 ± 0.16	0.40 ± 0.07	0.35 ± 0.04
Lung	9.33 ± 1.76	4.87 ± 0.54	2.29 ± 0.70	0.99 ± 0.12	0.73 ± 0.18
Kidney	17.89 ± 2.67	10.88 ± 2.28	3.36 ± 0.78	1.42 ± 0.25	1.00 ± 0.15

4.2.2. (E)-3-(4-Hydroxybenzylidene)-6-bromo-chroman-4-one (*3b*)

Yellow solid, mp 223–224 °C. Yield: 75%. ^{1}H NMR (DMSO-d_6) δ 7.92 (d, 1H, J = 2.7 Hz, H-5), 7.74–7.71 (m, 2H, H-7, =CHPh), 7.35 (d, 2H, J = 8.7 Hz, H-2′, H-6′), 7.06 (d, 1H, J = 8.7 Hz, H-8), 6.90 (d, 2H, J = 8.7 Hz, H-3′, H-5′), 5.45 (s, 2H, H-2). ^{13}C NMR ($CDCl_3$) δ 181.0, 160.1, 158.6, 138.8, 133.2, 131.3, 129.1, 127.5, 123.8, 121.2, 116.8, 115.4, 113.3, 68.2. HRMS: calcd for $C_{16}H_{11}^{79}BrO_3$ $[M]^+$ 329.9892, found 329.9896, calcd for $C_{16}H_{11}^{81}BrO_3$ $[M]^+$ 331.9871, found 331.9877. IR (KBr, cm^{-1}) γ 3163, 1655, 1602, 1284, 1020, 828.

4.2.3. (E)-3-Benzylidene-6-bromo-chroman-4-one (*3c*)

Gray solid, mp 143–144 °C. Yield: 80%. ^{1}H NMR ($CDCl_3$) δ 8.12 (s, 1H, H-5), 7.88 (s, 1H, =CHPh), 7.57–7.54 (m, 3H, H-7, H-2′, H-4′), 7.46–7.43 (m, 2H, H-3′, H-5′), 6.89–6.86 (m, 2H, H-8, H-4′), 5.35 (s, 2H, H-2). ^{13}C NMR ($CDCl_3$) δ 181.1, 159.8, 138.7, 135.5, 132.7, 130.5, 129.2, 128.4, 124.0, 122.3, 120.4, 115.2, 113.0, 68.5. HRMS: calcd for $C_{16}H_{11}^{79}BrO_2$ $[M]^+$ 313.9942, found 313.9946, calcd for $C_{16}H_{11}^{81}BrO_2$ $[M]^+$ 315.9922, found 315.9928. IR (KBr, cm^{-1}) γ 1675, 1607, 1472, 1283, 819.

4.2.4. (E)-3-(4-Dimethylamino-benzylidene)-6-bromo-chroman-4-one (*3d*)

Brown solid, mp 170–171 °C. Yield: 83%. ^{1}H NMR ($CDCl_3$) δ 8.11 (d, 1H, J = 2.4 Hz, H-5), 7.83 (s, 1H, =CHPh), 7.52 (dd, 1H, J = 2.4 Hz, 9.0 Hz, H-7), 7.25 (d, 2H, J = 8.4 Hz, H-2′, H-6′), 6.85 (d, 1H, J = 9.0 Hz, H-8), 6.72 (d, 2H, J = 8.4 Hz, H-3′, H-5′), 5.43 (s, 2H, H-2), 3.05 (s, 6H, NMe_2). ^{13}C NMR ($CDCl_3$) δ 180.9, 159.9, 151.6, 139.4, 138.0, 133.1, 130.4, 125.2, 124.0, 122.2, 120.0, 114.5, 112.0, 68.6, 40.3. HRMS: calcd for $C_{18}H_{16}^{79}BrNO_2$ $[M]^+$ 357.0364, found 357.0369, calcd for $C_{18}H_{16}^{81}BrNO_2$ $[M]^+$ 359.0344, found 359.0348. IR (KBr, cm^{-1}) γ 2984, 1657, 1600, 1288, 822.

4.2.5. (E)-3-(4-Nitrobenzylidene)-6-bromo-chroman-4-one (*3e*)

Yellow solid, mp 220–221 °C. Yield: 92%. ^{1}H NMR ($CDCl_3$) δ 8.31 (d, 2H, J = 8.7 Hz, H-3′, H-5′), 8.13 (d, 1H, J = 1.5 Hz, H-5), 7.88 (s, 1H, =CHPh), 7.60 (dd, 1H, J = 1.5 Hz, 8.7 Hz, H-7), 7.47 (d, 2H, J = 8.7 Hz, H-2′, H-6′), 6.91 (d, 1H, J = 8.7 Hz, H-8), 5.30 (s, 2H, H-2). ^{13}C NMR ($CDCl_3$) δ 180.8, 160.4, 140.8, 139.4, 135.6, 131.2, 130.9, 130.8, 130.8, 124.4, 123.6, 120.5, 115.4, 67.7. HRMS: calcd for $C_{16}H_{10}^{79}BrNO_4$ $[M]^+$ 358.9793, found 358.9795, calcd for $C_{16}H_{10}^{81}BrNO_4$ $[M]^+$ 360.9773, found 360.9779. IR (KBr, cm^{-1}) γ (3076), 1671, 1600, 1472, 1277, (1026), 823.

*4.2.6. (E)-3-(4-Bromobenzylidene)-6-bromo-chroman-4-one (**3g**)*

Gray solid, mp 162–163 °C. Yield: 78%. ^{1}H NMR ($CDCl_3$) δ 8.12 (d, 1H, J = 2.4 Hz, H-5), 7.80 (s, 1H, =CHPh), 7.61–7.53 (m, 3H, H-7, H-3′, H-5′), 7.18 (d, 2H, J = 8.4 Hz, H-2′, H-6′), 6.89 (d, 1H, J = 8.7 Hz, H-8), 5.30 (s, 2H, H-2). ^{13}C NMR ($CDCl_3$) δ 181.0, 160.2, 138.7, 137.6, 133.8, 133.2, 130.6, 124.9, 123.1, 122.5, 120.4, 115.3, 113.8, 68.1. HRMS: calcd for $C_{16}H_{10}Br_2O_2$ [M]$^+$ 393.9027, found 393.9024. IR (KBr, cm^{-1}) γ (3065), 1671, 1600, 1472, 1279, 1072, 823.

*4.2.7. (E)-3-(3-Bromo-4-dimethylamino-benzylidene)-6-bromo-chroman-4-one (**3h**)*

Yellow solid, mp 123–124 °C. Yield: 71%. ^{1}H NMR ($CDCl_3$) δ 8.09 (d, 1H, J = 2.4 Hz, H-5), 7.74 (s, 1H, =CHPh), 7.52 (dd, 1H, J = 8.4 Hz, 2.4 Hz, H-7), 7.50 (s, 1H, H-2′), 7.20 (d, 1H, J = 8.4 Hz, H-6′), 7.07 (d, 1H, J = 8.4 Hz, H-5′), 6.86 (d, 1H, J = 8.4 Hz, H-8), 5.35 (s, 2H, H-2), 2.89 (s, 6H, NMe_2). ^{13}C NMR ($CDCl_3$) δ 180.9, 160.1, 153.4, 138.7, 136.9, 136.3, 130.7, 130.6, 129.3, 129.2, 123.6, 120.3, 120.2, 118.1, 114.8, 68.1, 44.1. HRMS: calcd for $C_{18}H_{15}Br_2NO_2$ [M]$^+$ 436.9449, found 436.9442. IR (KBr, cm^{-1}) γ 2951, 2837, 1661, 1590, 1471, 1277, 819.

*4.2.8. (E)-3-(3,4-Dimethoxylbenzylidene)-6-bromo-chroman-4-one (**3i**)*

Pale brown solid, mp 175–176 °C. Yield: 65%. ^{1}H NMR ($CDCl_3$) δ 8.12 (s, 1H, H-5), 7.84 (s, 1H, =CHPh), 7.54–7.52 (m, 1H, H-7), 6.93–6.86 (m, 4H, H-8, H-2′, H-5′, H-6′), 5.39 (s, 2H, H-2), 3.94 (s, 3H, OMe), 3.91 (s, 3H, OMe). ^{13}C NMR ($CDCl_3$) δ 181.1, 160.0, 151.2, 150.5, 138.5, 132.7, 131.2, 128.3, 127.8, 123.6, 120.3, 119.6, 115.4, 114.7, 68.1, 55.6, 55.4. HRMS: calcd for $C_{18}H_{15}^{79}BrO_4$ [M]$^+$ 374.0154, found 374.0151, calcd for $C_{18}H_{15}^{81}BrO_4$ [M]$^+$ 376.0133, found 376.0128. IR (KBr, cm^{-1}) γ 2960, 2833, 1664, 1601, 1474, 1257, 817.

*4.2.9. (E)-3-(3-Methoxylbenzylidene)-6-bromo-chroman-4-one (**3j**)*

Pale brown solid, mp 108–109 °C. Yield: 81%. ^{1}H NMR ($CDCl_3$) δ 8.12 (s, 1H, H-5), 7.85 (s, 1H, =CHPh), 7.56 (d, 1H, J = 8.7 Hz, H-7), 7.40–7.35 (m, 1H, H-5′), 6.97 (d, 1H, J = 8.4 Hz, H-6′), 6.90–6.84 (m, 3H, H-2′, H-4′, H-8), 5.35 (s, 2H, H-2), 3.85 (s, 3H, OMe). ^{13}C NMR ($CDCl_3$) δ 181.3, 160.4, 160.1, 138.8, 138.6, 135.8, 130.7, 130.6, 130.2, 123.6, 122.7, 120.4, 115.9, 115.6, 114.9, 68.1, 55.7. HRMS: calcd for $C_{17}H_{13}^{79}BrO_3$ [M]$^+$ 344.0048, found 344.0046, calcd for $C_{17}H_{13}^{81}BrO_3$ [M]$^+$ 346.0028, found 346.0025. IR (KBr, cm^{-1}) γ 2986, 1675, 1618, 1271, 1062, 817.

*4.2.10. (E)-3-(3-Methoxyl-4-hydroxy-benzylidene)-6-bromo-chroman-4-one (**3k**)*

Pale brown solid, mp 115–116 °C. Yield: 67%. ^{1}H NMR ($CDCl_3$) δ 8.10 (s, 1H, H-5), 7.81 (s, 1H, =CHPh), 7.54 (d, 1H, J = 8.7 Hz, H-7), 6.98 (d, 1H, J = 8.1 Hz, H-6′), 6.87–6.81 (m, 3H, H-2′, H-5′, H-8), 5.98 (br, 1H, OH), 5.37 (s, 2H, H-2), 3.98 (s, 3H, OMe). ^{13}C NMR ($CDCl_3$) δ 181.1, 160.3, 152.8, 146.3, 138.7, 138.4, 136.0, 131.2, 130.2, 123.7, 122.8, 120.2, 116.1, 115.8, 115.0, 68.2, 55.9. HRMS: calcd for $C_{17}H_{13}^{79}BrO_4$ [M]$^+$ 359.9997, found 359.9992, calcd for $C_{17}H_{13}^{81}BrO_4$ [M]$^+$ 361.9977, found 361.9975. IR (KBr, cm^{-1}) γ 3488, 2969, 2847, 1669, 1589, 1517, 1472, 1264, 1035, 821.

*4.2.11. (E)-3-(4-Aminobenzylidene)-6-bromo-chroman-4-one (**3f**)*

Tin (II) chloride (3.08 mmol) was added to a solution of (*E*)-3-(4-nitrobenzylidene)-6-bromo-chroman-4-one (**3e**) (0.61 mmol) in ethanol (25 mL). The reaction mixture was refluxed under nitrogen for 4 h and then cooled to room temperature. After ethanol was evaporated, 1 M NaOH was added until the mixture became basic (pH 8–9). After extraction with ethyl acetate (50 mL × 2), the combined organic layers were washed with brine, dried over anhydrous Na_2SO_4 and filtered. The solvent was removed, and the residue was purified by silica gel chromatography (2:1 petroleum ether/ethyl acetate) to give **3f** as a pale brown solid. Yield: 52%. Mp 186–187 °C. ^{1}H NMR (DMSO-d_6) δ 7.95 (s, 1H, H-5), 7.88 (s, 1H, =CHPh), 7.75–7.72 (m, 1H, H-7), 7.21 (d, 2H, J = 8.4 Hz, H-2′, H-6′), 7.10–7.07 (m, 1H, H-8), 6.65 (d, 2H, J = 8.4 Hz, H-3′, H-5′), 5.45 (s, 2H, H-2). ^{13}C NMR ($CDCl_3$) δ 180.9, 159.8, 148.5, 139.0, 138.7, 134.1, 130.8, 126.4, 124.0, 122.2, 120.8, 115.5, 113.7, 68.3. HRMS: calcd for $C_{16}H_{12}^{79}BrNO_2$ [M]$^+$ 329.0051, found 329.0058, calcd for $C_{16}H_{12}^{81}BrNO_2$ [M]$^+$ 331.0031, found 331.0034. IR (KBr, cm^{-1}) γ 3383, 2962, 1671, 1600, 1472, 1276, 1024, 816.

*4.2.12. (E)-3-(3,5-Dimethoxylbenzylidene)-6-bromo-chroman-4-one (**3l**)*

To the suspension of 6-bromo-chromosome **1** (1.35 mmol) in acetic acid (2.1 mL) was added HCl (0.38 mL). After 10 min, 3, 5-dimethoxyl benzaldehyde **2l** (1.35 mmol) was added with stirring. Then the mixture was stirred for 2 h at room temperature, and placed for 2 d. It was treated with saturated aqueous Na_2CO_3 until alkaline, and the precipitate was filtered to give a brown solid. The crude product obtained was subjected to column chromatography on silica gel (CH_2Cl_2/methanol = 20/1) to give **3l**. Yield: 53%. ^{1}H NMR ($CDCl_3$) δ 8.11 (s, 1H, H-5), 7.80 (s, 1H, =CHPh), 7.56–7.54 (m, 1H, H-7), 6.87 (d, 1H, J = 8.7 Hz, H-8), 6.51 (s, 1H, H-4′), 6.42 (s, 2H, H-2′, H-6′), 5.33 (s, 2H, H-2), 3.84 (s, 6H, OMe). ^{13}C NMR ($CDCl_3$) δ 181.3, 161.1, 160.3 (2C), 138.8, 138.7, 136.1, 130.7, 130.6, 123.5, 120.4, 114.8, 108.2 (2C), 101.8, 68.1, 55.8. HRMS: calcd for $C_{18}H_{15}^{79}BrO_4$ [M]$^+$ 374.0154, found 374.0150, calcd for $C_{18}H_{15}^{81}BrO_4$ [M]$^+$ 376.0133, found 376.0128. IR (KBr, cm^{-1}) γ 2960, 2935, 2837, 1670, 1597, 1474, 1274, 825.

4.3. Iododestannylation reaction

(*E*)-3-(4-Dimethylamino-benzylidene)-6-tributylstannyl-chroman-4-one (**3m**). A mixture of **3d** (286 mg, 0.87 mmol), bis(-tributyltin) (0.55 mL), and $(Ph_3P)_4Pd$ (41 mg, 0.035 mmol) in triethylamine (28 mL) was stirred at 90 °C for 6 h. The solvent was removed, and the residue was purified by silica gel chromatography (6:1 hexane/ethyl acetate) to give 174 mg of **3m**. Yield: 28%. ^{1}H NMR (300 MHz, $CDCl_3$) δ 8.09 (s, 1H, H-5), 7.82 (s, 1H, =CHPh), 7.56–7.53 (m, 1H, H-7), 7.27–7.25 (d, 2H, J = 8.4 Hz, H-2′, H-6′), 6.95–6.92 (m, 1H, H-8), 6.73–6.71 (d, 2H, J = 8.4 Hz, H-3′, H-5′), 5.41 (s, 2H, H-2), 3.04 (s, 6H, NMe_2), 1.55–1.51 (m, 6H, $-CH_2Sn$), 1.35–1.32 (m, 6H, $-CH_2CH_2Sn$), 1.09–1.06 (m, 6H, $-CH_2CH_2CH_2Sn$), 0.90–0.88 (m, 9H, CH_3).

The radioiodinated form of compound **3d** was prepared from the corresponding tributyltin precursor **3m** by iododestannylation reaction. Briefly, to initiate the reaction, 100 μL of H_2O_2 (3%) was added to a mixture of the tributyltin derivative (100 μg in 100 μL of EtOH), 1.5 mCi sodium [^{125}I]iodide (specific activity 2200 Ci/mmol), and 100 μL of 1 N HCl in a sealed vial. The reaction was allowed to proceed at room temperature for 10 min and terminated by addition of $NaHSO_3$. The reaction, after neutralization with sodium bicarbonate, was extracted with ethyl acetate. The extract was dried by passing through an anhydrous Na_2SO_4 column and was then blown to dryness with a stream of nitrogen gas. The radioiodinated ligand was purified by HPLC (Column: Waters Symmetry C18, 4.6 × 250 mm, 5 μm; Mobile phase: MeOH/H_2O = 8/2; Flow rate = 1.0 mL/min). The purified ligand was stored at −20 °C for the biodistribution study.

4.4. Biological evaluation

4.4.1. Binding assay in vitro using Aβ aggregates

Inhibition experiments were carried out in 12 × 75 mm borosilicate glass tubes according to procedures described previously

with some modifications. Briefly, 100 μL of aggregated $A\beta_{1-40}$ fibrils (60 nM in the final assay mixture) was added to a mixture containing 100 μL of radioligands ([^{125}I]IMPY) at an appropriate concentration, 100 μL of inhibitors ($3 \times 10^{-6} - 1 \times 10^{-10}$ M in EtOH) and 700 μL of PBS (0.2 M, pH = 7.4) in a final volume of 1 mL. The mixture was incubated at 37 °C for 2 h, and then the bound and free radioactive fractions were separated by vacuum filtration through borosilicate glass fiber filters (Whatman GF/B) using a ZT-II-12R cell harvester (Satellite Medical Equipment, Shaoxing, China) followed by 3 × 3 mL washes of ice-cold PBS. The radioactivity from filters containing the bound ^{125}I ligand was measured in a γ-counter (PerkinElmer Life, WALLAC/Wizard 1470, USA) with a 70% counting efficiency. The half maximal inhibitory concentration (IC_{50}) was determined from displacement curve of three independent experiments using GraphPad Prism 5.0, and the inhibition constant (K_i) was calculated using the Cheng–Prusoff equation: $K_i = IC_{50}/(1 + [L]/K_d)$, where [$L$] is the concentration of radioligand used in the assay, and K_d is the dissociation constant of the radioligand.

4.4.2. AD brain tissue fluorescent staining

Brain tissues were obtained from autopsy-confirmed AD subjects. Adjacent tissue sections (6 μm thickness) were processed for staining. Firstly, the paraffin brain sections were treated with 2 × 10 min washes in xylene, 2 × 10 min washes in 100% ethanol, 5 min sequential washes in 95%, 90%, 80% and 70% ethanol, and sequential rinsings (5 min each) in milli-Q water and phosphate buffered saline (0.01 M PBS, pH 7.4). Secondly, to quench the autofluorescence, the sections were blanched in 0.25% potassium permanganate solution for 20 min, washed in PBS and treated with 0.1% potassium metabisulfite and 0.1% oxalic acid in PBS, followed by washing in PBS. The quenched brain tissue sections were immersed in a solution of cold ligand (50 μM in 30% EtOH in 0.1 M PBS, 20 min), ThS (1% in milli-Q water, 5 min). Thirdly, the sections were differentiated by 50% EtOH/H_2O for 10 min (cold ligand), or 70% EtOH/H_2O for 10 min (ThS). Finally, the sections were washed in PBS (3 × 5 min) and sealed with 80% glycerin/PBS and coverslips. These sections were stored at 4 °C in darkness and viewed using an Olympus IX71 fluorescence microscope (Olympus, Tokyo) with an SPOT digital camera (Diagnostic Instruments, Detroit, MI).

4.4.3. In vivo biodistribution in normal mice

Animal studies were conducted in accordance with our institutional guidelines and were approved by the Animal Care Committee of Hefei University of Technology. A saline solution (0.9%, 100 μL) containing the radiolabeled agent [^{125}I]**3n** (2 μCi) was injected directly into the tail vein of ICR mice (5 weeks old, average weight of 25–30 g). The mice ($n = 5$ for each time point) were euthanized at predetermined time points (2, 10, 30, 60, 120 min). The organs of interest were removed and weighed, and the radioactivity was counted with an automatic gamma counter. The tissue radioactivity concentrations (% ID/g) were calculated by dividing the sample counts per gram of tissue by the counts from 1% of the initially injected dose (100-fold diluted aliquots of the injected material).

Acknowledgments

We are grateful to the Key Laboratory of Brain Function and Disease, Chinese Academy of Sciences (No. 2012-2) for financial support.

Appendix A. Supplementary data

Supplementary data related to this article can be found at http://dx.doi.org/10.1016/j.ejmech.2014.02.020.

References

[1] D.J. Selkoe, Alzheimer disease: mechanistic understanding predicts novel therapies, Annals of Internal Medicine 140 (2004) 627–638.
[2] H.W. Querfurth, F.M. LaFerla, Mechanisms of disease: Alzheimer's disease, The New England Journal of Medicine 362 (2010) 329–344.
[3] P.J. Nestor, P. Scheltens, J.R. Hodges, Advances in the early detection of Alzheimer's disease, Nature Medicine 10 (Suppl.) (2004) S34–S41.
[4] E.D. Roberson, L. Mucke, 100 years and counting: prospects for defeating Alzheimer's disease, Science 314 (2006) 781–784.
[5] A. Nordberg, PET imaging of amyloid in Alzheimer's disease, The Lancet Neurology 3 (2004) 519–527.
[6] A. Nordberg, The future: new methods of imaging exploration in Alzheimer's disease, Frontiers of Neurology and Neuroscience 24 (2009) 47–53.
[7] C.A. Mathis, Y. Wang, D.P. Holt, G. Huang, M.L. Debnath, W.E. Klunk, Synthesis and evaluation of ^{11}C-labeled 6-substituted 2-arylbenzothiazoles as amyloid imaging agents, Journal of Medicinal Chemistry 46 (2003) 2740–2754.
[8] W.E. Klunk, H. Engler, A. Nordberg, Y. Wang, G. Blomqvist, D.P. Holt, M. Bergstrom, I. Savitcheva, G.F. Huang, S. Estrada, B. Ausen, M.L. Debnath, J. Barletta, J.C. Price, J. Sandell, B.J. Lopresti, A. Wall, P. Koivisto, G. Antoni, C.A. Mathis, B. Langstrom, Imaging brain amyloid in Alzheimer's disease with Pittsburgh compound-B, Annals of Neurology 55 (2004) 306–319.
[9] C.C. Rowe, S. Ng, U. Ackermann, S.J. Gong, K. Pike, G. Savage, T.F. Cowie, K.L. Dickinson, P. Maruff, D. Darby, C. Smith, M. Woodward, J. Merory, H. Tochon-Danguy, G. O'Keefe, W.E. Klunk, C.A. Mathis, J.C. Price, C.L. Masters, V.L. Villemagne, Imaging beta-amyloid burden in aging and dementia, Neurology 68 (2007) 1718–1725.
[10] N.P. Verhoeff, A.A. Wilson, S. Takeshita, L. Trop, D. Hussey, K. Singh, H.F. Kung, M.P. Kung, S. Houle, In vivo imaging of Alzheimer disease beta-amyloid with [^{11}C]SB-13 PET, The American Journal of Geriatric Psychiatry 12 (2004) 584–595.
[11] A.E. Johnson, F. Jeppsson, J. Sandell, D. Wensbo, J.A. Neelissen, A. Jureus, P. Strom, H. Norman, L. Farde, S.P. Svensson, AZD2184: a radioligand for sensitive detection of β-amyloid deposits, Journal of Neurochemistry 108 (2009) 1177–1186.
[12] K. Shoghi-Jadid, G.W. Small, E.D. Agdeppa, V. Kepe, L.M. Ercoli, P. Siddarth, S. Read, N. Satyamurthy, A. Petric, S.C. Huang, J.R. Barrio, Localization of neurofibrillary tangles and beta-amyloid plaques in the brains of living patients with Alzheimer disease, The American Journal of Geriatric Psychiatry 10 (2002) 24–35.
[13] J.R. Barrio, N. Satyamurthy, S.C. Huang, A. Petric, G.W. Small, V. Kepe, Dissecting molecular mechanisms in the living brain of dementia patients, Accounts of Chemical Research 42 (2009) 842–850.
[14] M. Koole, D.M. Lewis, C. Buckley, N. Nelissen, M. Vandenbulcke, D.J. Brooks, R. Vandenberghe, K. Van Laere, Whole-body biodistribution and radiation dosimetry of ^{18}F-GE067: a radioligand for in vivo brain amyloid imaging, Journal of Nuclear Medicine 50 (2009) 818–822.
[15] C.C. Rowe, U. Ackerman, W. Browne, R. Mulligan, K.L. Pike, G. O'Keefe, H. Tochon-Danguy, G. Chan, S.U. Berlangieri, G. Jones, K.L. Dickinson-Rowe, H.P. Kung, W. Zhang, M.P. Kung, D. Skovronsky, T. Dyrks, G. Holl, S. Krause, M. Friebe, L. Lehman, S. Lindemann, L.M. Dinkelborg, C.L. Masters, V.L. Villemagne, Imaging of amyloid beta in Alzheimer's disease with [^{18}F]BAY94-9172, a novel PET tracer: proof of mechanism, The Lancet Neurology 7 (2008) 129–135.
[16] S.R. Choi, G. Golding, Z. Zhuang, W. Zhang, N. Lim, F. Hefti, T.E. Benedum, M.R. Kilbourn, D. Skovronsky, H.F. Kung, Preclinical properties of ^{18}F-AV-45: a PET imaging agent for Aβ plaques in the brain, Journal of Nuclear Medicine 50 (2009) 1887–1894.
[17] H.F. Kung, S.R. Choi, W. Qu, W. Zhang, D. Skovronsky, ^{18}F Stilbenes and styrylpyridines for PET imaging of Aβ plaques in Alzheimer's disease, Journal of Medicinal Chemistry 53 (2010) 933–941.
[18] A.B. Newberg, N.A. Wintering, K. Plossl, J. Hochold, M.G. Stabin, M. Watson, D. Skovronsky, C.M. Clark, M.P. Kung, H.F. Kung, Safety, biodistribution, and dosimetry of ^{123}I-IMPY: a novel amyloid plaque-imaging agent for the diagnosis of Alzheimer's disease, Journal of Nuclear Medicine 47 (2006) 748–754.
[19] Y. Kudo, N. Okamura, S. Furumoto, M. Tashiro, K. Furukawa, M. Maruyama, M. Itoh, R. Iwata, K. Yanai, H. Arai, 2-(2-[2-Dimethylaminothiazol-5-yl]ethenyl)-6-(2-[fluoro]ethoxy)benzoxazole: a novel PET agent for in vivo detection of dense amyloid plaques in Alzheimer's disease patients, Journal of Nuclear Medicine 48 (2007) 553–561.
[20] R. Vandenberghe, K. Van Laere, A. Ivanoiu, E. Salmon, C. Bastin, E. Triau, S. Hasselbalch, I. Law, A. Andersen, A. Korner, L. Minthon, G. Garraux, N. Nelissen, G. Bormans, C. Buckley, R. Owenius, L. Thurfjell, G. Farrar, D.J. Brooks, ^{18}F-flutemetamol amyloid imaging in Alzheimer disease and mild cognitive impairment: a phase 2 trial, Annals of Neurology 68 (2010) 319–329.
[21] C.C. Rowe, V.L. Villemagne, Brain amyloid imaging, Journal of Nuclear Medicine 52 (2011) 1733–1740.
[22] V.L. Villemagne, C.C. Rowe, Amyloid imaging, International Psychogeriatrics 23 (Suppl. 2) (2011) S41–S49.
[23] M.P. Kung, C. Hou, Z.P. Zhuang, A.J. Cross, D.L. Maier, H.F. Kung, Characterization of IMPY as a potential imaging agent for beta-amyloid plaques in double transgenic PSAPP mice, European Journal of Nuclear Medicine and Molecular Imaging 31 (2004) 1136–1145.

[24] M.P. Kung, C. Hou, Z.P. Zhuang, B. Zhang, D. Skovronsky, J.Q. Trojanowski, V.M. Lee, H.F. Kung, IMPY: an improved thioflavin-T derivative for in vivo labeling of beta-amyloid plaques, Brain Research 956 (2002) 202–210.
[25] Z.P. Zhuang, M.P. Kung, A. Wilson, C.W. Lee, K. Plossl, C. Hou, D.M. Holtzman, H.F. Kung, Structure-activity relationship of imidazo[1,2-α]pyridines as ligands for detecting beta-amyloid plaques in the brain, Journal of Medicinal Chemistry 46 (2003) 237–243.
[26] M.P. Kung, C. Hou, Z.P. Zhuang, D. Skovronsky, H.F. Kung, Binding of two potential imaging agents targeting amyloid plaques in postmortem brain tissues of patients with Alzheimer's disease, Brain Research 1025 (2004) 98–105.
[27] H.J. Heo, C.Y. Lee, Protective effects of quercetin and vitamin C against oxidative stress-induced neurodegeneration, Journal of Agricultural and Food Chemistry 52 (2004) 7514–7517.
[28] K. Ono, Y. Yoshiike, A. Takashima, K. Hasegawa, H. Naiki, M. Yamada, Potent anti-amyloidogenic and fibril-destabilizing effects of polyphenols in vitro: implications for the prevention and therapeutics of Alzheimer's disease, Journal of Neurochemistry 87 (2003) 172–181.
[29] M. Ono, N. Yoshida, K. Ishibashi, M. Haratake, Y. Arano, H. Mori, M. Nakayama, Radioiodinated flavones for in vivo imaging of β-amyloid plaques in the brain, Journal of Medicinal Chemistry 48 (2005) 7253–7260.
[30] M. Ono, Y. Maya, M. Haratake, M. Nakayama, Synthesis and characterization of styrylchromone derivatives as beta-amyloid imaging agents, Bioorganic & Medicinal Chemistry 15 (2007) 444–450.
[31] T. Al Nakib, V. Bezjak, M.J. Meegan, R. Chandy, Synthesis and antifungal activity of some 3-benzylidenechroman-4-ones, 3-benzylidenethiochroman-4-ones and 2-benzylidene-1-tetralones, European Journal of Medicinal Chemistry 25 (1990) 455–462.
[32] S. Tait, A.L. Salvati, N. Desideri, L. Fiore, Antiviral activity of substituted homoisoflavonoids on enteroviruses, Antiviral Research 72 (2006) 252–255.
[33] E. Miadokova, I. Masterova, V. Vlckova, V. Duhova, J. Toth, Antimutagenic potential of homoisoflavonoids from *Muscari racemosum*, Journal of Ethnopharmacology 81 (2002) 381–386.
[34] V. Siddaiah, M. Maheswara, C.V. Rao, S. Venkateswarlu, G.V. Subbaraju, Synthesis, structural revision, and antioxidant activities of antimutagenic homoisoflavonoids from *Hoffmanosseggia intricata*, Bioorganic & Medicinal Chemistry Letters 17 (2007) 1288–1290.
[35] S. Kirkiacharian, H.G. Tongo, J. Bastide, P. Bastide, M.M. Grenie, Synthèse et activités angioprotectrice, anti-allergique et antihistaminique de benzyl-3 chromones (homo-isoflavones), European Journal of Medicinal Chemistry 24 (1989) 541–546.
[36] T.M. Hung, C.V. Thu, N.T. Dat, S.W. Ryoo, J.H. Lee, J.C. Kim, M. Na, H.J. Jung, K. Bae, B.S. Min, Homoisoflavonoid derivatives from the roots of *Ophiopogon japonicus* and their in vitro anti-inflammation activity, Bioorganic & Medicinal Chemistry Letters 20 (2010) 2412–2416.
[37] L.G. Lin, H. Xie, H.L. Li, L.J. Tong, C.P. Tang, C.Q. Ke, Q.F. Liu, L.P. Lin, M.Y. Geng, H. Jiang, W.M. Zhao, J. Ding, Y. Ye, Naturally occurring homoisoflavonoids function as potent protein tyrosine kinase inhibitors by c-Src-based high-throughput screening, Journal of Medicinal Chemistry 51 (2008) 4419–4429.
[38] N. Desideri, A. Bolasco, R. Fioravanti, L.P. Monaco, F. Orallo, M. Yáñez, F. Ortuso, S. Alcaro, Homoisoflavonoids: natural scaffolds with potent and selective monoamine oxidase-b inhibition properties, Journal of Medicinal Chemistry 54 (2011) 2155–2164.
[39] Y. Sun, J. Chen, X. Chen, L. Huang, X. Li, Inhibition of cholinesterase and monoamine oxidase-B activity by Tacrine–Homoisoflavonoid hybrids, Bioorganic & Medicinal Chemistry 21 (2013) 7406–7417.
[40] A. Manook, B.H. Yousefi, A. Willuweit, S. Platzer, S. Reder, et al., Small-animal PET imaging of amyloid-beta plaques with [^{11}C]PiB and its multi-modal validation in an APP/PS1 mouse model of Alzheimer's disease, PLoS ONE 7 (2012) e31310, http://dx.doi.org/10.1371/journal.pone.0031310.
[41] B. Neumaier, S. Deisenhofer, C. Sommer, C. Solbach, S.N. Reske, F. Mottaghy, Synthesis and evaluation of ^{18}F-fluoroethylated benzothiazole derivatives for in vivo imaging of amyloid plaques in Alzheimer's disease, Applied Radiation and Isotopes 68 (2010) 1066–1072.
[42] B.H. Yousefi, A. Drzezga, B. von Reutern, A. Manook, M. Schwaiger, H.J. Wester, G. Henriksen, A novel ^{18}F-labeled imidazo[2,1-*b*]benzothiazole (IBT) for high-contrast PET imaging of β-amyloid plaques, ACS Medicinal Chemistry Letters 2 (2011) 673–677.
[43] J.P. Qiao, C.S. Gan, C.W. Wang, J.F. Ge, D.D. Nan, J. Pan, J.N. Zhou, Novel indanone derivatives as potential imaging probes for β-amyloid plaques in the brain, ChemBioChem 13 (2012) 1652–1662.
[44] D.N. Kevill, E.D. Weiler, N.H. Cromwell, Cis–trans isomerism of exocyclic α,β-unsaturated indanones and tetralones, The Journal of Organic Chemistry 29 (1964) 1276–1278.